



HAL
open science

Exploiting internal resonances in nonlinear structures with cyclic symmetry as a mean of passive vibration control

Samuel Quaegebeur, N. Di Palma, B. Chouvion, Fabrice Thouverez

► **To cite this version:**

Samuel Quaegebeur, N. Di Palma, B. Chouvion, Fabrice Thouverez. Exploiting internal resonances in nonlinear structures with cyclic symmetry as a mean of passive vibration control. *Mechanical Systems and Signal Processing*, 2022, 178, pp.109232. 10.1016/j.ymssp.2022.109232 . hal-04081505

HAL Id: hal-04081505

<https://hal.science/hal-04081505>

Submitted on 29 Aug 2023

HAL is a multi-disciplinary open access archive for the deposit and dissemination of scientific research documents, whether they are published or not. The documents may come from teaching and research institutions in France or abroad, or from public or private research centers.

L'archive ouverte pluridisciplinaire **HAL**, est destinée au dépôt et à la diffusion de documents scientifiques de niveau recherche, publiés ou non, émanant des établissements d'enseignement et de recherche français ou étrangers, des laboratoires publics ou privés.

Exploiting internal resonances in nonlinear structures with cyclic symmetry as a mean of passive vibration control

Samuel Quaegebeur^{a,b,*}, Nicolas Di Palma^b, Benjamin Chouvion^c, Fabrice Thouverez^b

^a*Safran Helicopter Engines, 64511 Bordes, France*

^b*Ecole Centrale de Lyon, LTDS UMR 5513, 69130 Ecully, France*

^c*Centre de recherche de l'école de l'air, Ecole de l'air et de l'espace, 13661, Salon-de-Provence*

Abstract

The purpose of this paper is to study how internal resonances can be used to mitigate the vibration of cyclically symmetric systems exhibiting geometrical nonlinear effects. The method of multiple scales is employed to derive specific conditions that allow such energy transfers. This novelty is confirmed through numerical investigations, and an application to decrease the vibration of the system is proposed. A simplified yet realistic blade model with geometrical nonlinearities is considered. It includes pre-twist, pre-bending and warping, and is duplicated to create a full bladed rotor with cyclically symmetric properties. As the model of the whole structure may become large, it is further reduced via the normal form approach. The harmonic balance method is then employed to obtain periodic solutions, localize bifurcation points and then follow bifurcated branches. These numerical solutions are used in complement with the aforementioned theoretical conditions to investigate the energy transfer properties of the mechanical system. Through these simulations, an effective range of amplitude excitation is defined to obtain internal resonances leading to an overall vibration mitigation of the system.

Keywords: Internal resonance, Normal form theory, Geometric nonlinearities, Multiple scale analysis, Harmonic Balance Method, Bifurcation analysis

1. Introduction

Over the years, different processes exploiting effects of nonlinearities have been used to reduce the vibrations of mechanical structures. Adding friction devices [1] allows to damp the motion of the system but leads to wear which inevitably decreases the efficiency of this method. Nonlinear energy sinks [2, 3] consist

*Corresponding author

Email address: samuel.quaegebeur@ec-lyon.fr (Samuel Quaegebeur)

5 in attaching a small mass to the main structure (host) with a nonlinear stiffness. The vibration of the host is mitigated as its energy is transferred to the secondary system. The main limitation of this technique is that the exchange occurs for a relatively narrow range of excitation, which is however still more efficient than a linear tuned absorber designed to accommodate a single resonant peak. To remedy this issue, nonlinear tuned vibrations absorbers have been defined [4, 5]. These devices show promising results but are complicated to
10 implement in practise in a complex engineered structure. The main motivation behind the current paper is to use the intrinsic nonlinear features of the structure (i.e without adding external masses) to mitigate its vibrational levels. The focus is made on the use of internal resonances as a possible mean of vibration control.

To decrease their environmental impact, turboengines tend to have larger diameters while maintaining a
15 slender profile. This design leads to more pronounced geometrical nonlinear effects of the fan. Nonlinearities may lead to localization effects [6] but also to internal resonances [7]. This latter nonlinear process corresponds to a transfer of energy between different modes. The book of Nayfeh and Mook [7] proposed several approaches to study internal resonances. One popular analytical method is the multiple scales approach. It consists in seeking the displacement as a function of multiple independent variables. This expansion is
20 performed up to a specific order. It has been employed for systems with geometrical nonlinearities with a second order [7] and a third order expansions [8]. Monteil et al. used this approach to study a cascade of interactions [9]. Recent work of Gobat et al. focused on an 1:2 internal resonance and quasiperiodic regimes [10]. They also presented experimental evidence of this phenomenon with gyroscopic effects [11].

In recent work [12], parameters controlling the appearance of a 1:2 internal resonance (between the
25 second bending mode and the first torsional mode) in a blade with geometrical nonlinearities have been identified. The blade was modeled as a sophisticated beam with important features of large blade design used in turbomachinery manufacturers, such as pre-twist, pre-bending, and warping.

While the investigation of internal resonances is abundant for a single blade or beam, there has been very few researches on this subject for cyclically symmetric structures. Pioneer work was first proposed by
30 Vakakis et al. [13, 14, 15] and describes the mode localization in such structures. Computation of multiple solutions has also been considered in [16, 17, 18]. The paper of Georgiades et al. [19] describes the modal interaction occurring in cyclic systems and shows that energy transfer may occur even if the frequencies of the modes are incommensurable. In [20], it was proposed to determine the nonlinear interaction occurring in cyclic systems when specific nodal diameters were excited. The main purpose was to identify a reduced set
35 of interacting nodal diameters, to create a reduced-order model (ROM), and to express the nonlinear forces

in the cyclic domain. Such reduction allowed to decrease significantly the computation time and enabled to find some internal resonances. These aforementioned papers show that energy transfer in nonlinear structures with cyclic symmetry is of current interest in the scientific community. However, it feels that the subject remains incomplete: to better control the energy transfer in such structures, one must be able to predict with confidence the configurations for which internal resonances may occur. This issue is tackled in this paper in which analytical derivations are proposed via the multiple scales approach to determine the conditions required to obtain internal resonances in cyclically symmetric systems. In this paper, it is demonstrated as a practical example how the transversal displacement of a cyclic structure can be reduced through an 1:2 internal resonance. The analytical relations are verified numerically by extending the blade design developed in [12] to a cyclically symmetric system. Due to the large size of the system and the numerical analysis proposed (including stability analysis, branch switching, and bifurcations points tracking), a reduced-order model must be used. The normal form theory [21, 22] which relies on the Poincare-Dulac's theorem [23] was chosen as reduction methodology.

The present paper differs from [20] because the analysis performed here accounts for all the nodal diameters, whereas a reduction was performed in [20]. This allows to predict all possible internal resonances and this could not have been obtained with the approach proposed in [20].

Section 2 presents the mechanical model, its reduction and the numerical algorithms employed in the remaining of the paper. The numerical and reduction tools are validated in Section 3 by studying the dynamics of a single sector. Section 4 shows how the multiple scales approach can provide some theoretical conditions to obtain 1:2 internal resonances in cyclically symmetric systems. These theoretical results are then verified numerically in Section 5. Finally, Section 6 complicates the problem further and proposes an application to decrease the energy of the system by exploiting the internal resonance as a passive vibration control.

2. Presentation of the model and the numerical tools used for its simulation

In this article, we study a simplified model of a rotor composed of N blades with geometrical nonlinearities. This section first briefly recalls the construction of the realistic blade model which was presented in [12] before explaining its extension to a cyclic structure. As the size of the model and the number of nonlinear degrees of freedom can get large, a reduced-order model based on the normal form theory [24, 21] will also be employed.

2.1. Nonlinear pre-bent blade model with an initial twist

65 The simplified nonlinear blade model used is similar to the one derived in [12], in which the authors combined the work of [25] and [26]. Although only the centerline of the beam is considered, the construction includes all key design features of a blade such as possible pre-bending (defined with the function z_e), a variable twist along the length of the blade (accounted for via a change of coordinates, see Figure 1), and warping of the cross-section. The geometrical nonlinearities are derived from the potential energy of the system. The blade is supposed to be clamped at one end and free at its tip.

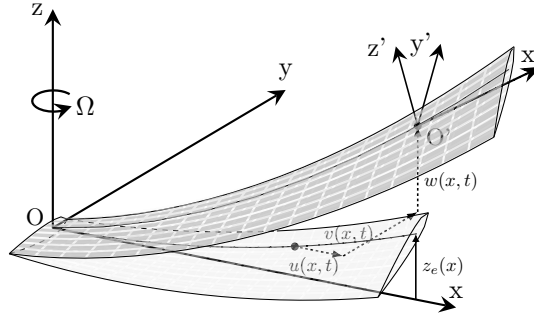


Figure 1: Representation of the pre-bent and twisted blade.

In [12], a Rayleigh-Ritz discretization was performed. To facilitate the assembly of the blades and the creation of the cyclically symmetric system that will be used in Section 5, the finite-element method is here employed. Hermitian polynomials [27] with eight degrees of freedom per node are used. The degrees of freedom characterize u (displacement along \vec{x}'), v (displacement along \vec{y}'), w (displacement along \vec{z}'), ϕ (torsion angle along \vec{x}) and their derivatives along the curvilinear abscissa.

The first three modes of the system are given in Table 1. They are similar to the ones obtained in [12]. As the natural frequency of the second flexural mode, ω_2 , is close to twice the natural frequency of the first torsional mode, ω_1 , ($\omega_2 \approx 2\omega_1$), an 1:2 internal resonance may occur between these two modes [28]. This exchange of energy was studied in [12]. It was shown that by exciting the second flexural mode with a sufficiently high external force, a bifurcated branch appears and couples the first torsional mode. In our study, the same mode is excited: an harmonic forced with frequency taken in the vicinity of ω_2 is applied at the tip of the blade along the transversal axis.

Frequencies	Associated deformed shapes
$\omega_0 = 71.6 \text{ rad s}^{-1}$	First flexural mode (1F)
$\omega_1 = 221.2 \text{ rad s}^{-1}$	First torsional mode (1T)
$\omega_2 = 443.0 \text{ rad s}^{-1}$	Second flexural mode (2F)

Table 1: Natural frequencies of the first three modes of the single blade system.

2.2. Extension to cyclically symmetric systems

We now extend this simple blade model to a cyclically symmetric system with N sectors (N blades).
 85 Our model may simulate relatively complex geometry such as the one illustrated in Figure 2a. Each blade
 is discretized into 5 elements. All the blades are clamped to a rigid disk. Linear stiffnesses attached to the
 second node of each blade, as represented in Figure 2, are added to model the relative disk flexibility. In
 order to maintain the possible appearance of internal resonances, the values of the stiffnesses are taken to
 be small so as not to influence too much the natural frequencies. A similar cyclic structure with coupling
 90 stiffnesses was also employed in [17]. However, the blade model is here much more realistic and can also
 exhibit internal resonances.

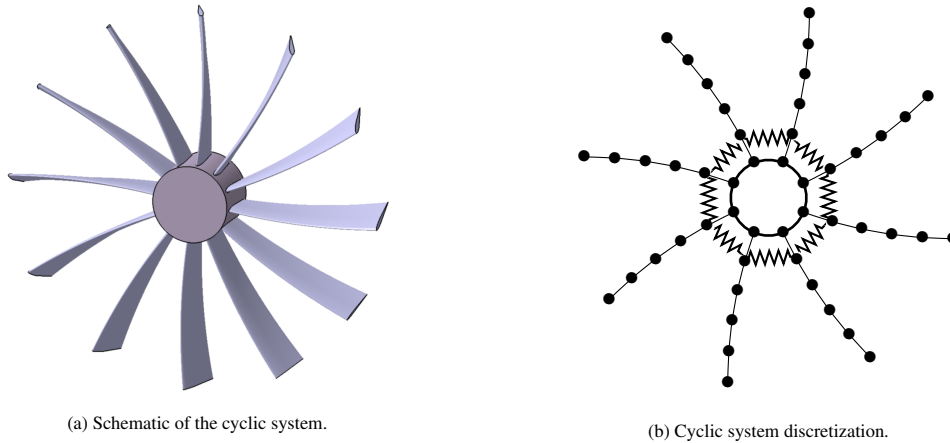


Figure 2: Different levels of representation of a cyclically symmetric system.

For the case of $N = 5$, Figure 3 illustrates the first natural frequencies calculated for each nodal diameter. We observe that multiple internal resonances can occur. If we were to excite the structure around the second bending mode of the nodal diameter 0 (denoted ND0), then modal interaction between this excited mode

95 and the second bending mode of ND1 and ND2 (i.e 1:1 internal resonances may occur), as well as between the excited mode and the first torsional mode of ND0, ND1, and ND2 (i.e 1:2 internal resonances).

In the next sections, a traveling wave excitation is applied in the transverse direction at the tip of the blades with an engine order equal to m , varying between $\llbracket 0, K \rrbracket$ where $K = \frac{N}{2}$ if N is even or $K = \frac{N-1}{2}$ otherwise [29, 30].

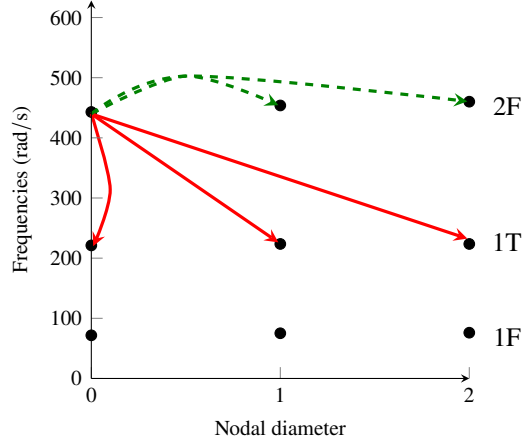


Figure 3: First three natural frequencies of each nodal diameter for $N = 5$. The full red lines with arrows, \rightarrow , denote potential 1:2 internal resonances. The dashed green lines, $- -$, denote possible 1:1 internal resonance.

100 2.3. Reduction by the normal form theory

Without reduction, the full structure, discretized by finite elements, contains $N_{\text{dof}} \times N$ coupled nonlinear unknowns, where N_{dof} , the number of degrees of freedom for a single sector, is already equal to 42 when 5 elements are used per blade. In order to decrease the computation time of the following numerical simulations, a reduced-order model obtained with the normal form theory is used. In this paper, a damped motion of the system is considered, and hence the approach of Touzé and Amabili [21] is well suited. Their reduction methodology is applied to both a single blade (Section 2.3.1) and the full cyclically symmetric system (Section 2.3.2). This particular choice of reduction methodology was arbitrary and another one could have been applied (such as the modal derivatives [31, 32], subspectral manifold [33], or dual modes [34]). A recent literature review [22] presents these different methods.

The analytical development is first explained for the single blade system whose equation of motion after discretization can be written as

$$\mathbf{M}\ddot{\mathbf{u}} + \mathbf{C}\dot{\mathbf{u}} + \mathbf{K}\mathbf{u} + \mathbf{f}_{\text{nl}}(\mathbf{u}) = \mathbf{f}_{\text{ext}}, \quad (1)$$

where \mathbf{M} , \mathbf{C} , and \mathbf{K} are the mass, damping and stiffness matrices. \mathbf{C} is here defined as modal damping such that the second flexural mode and the first torsional mode both have a damping of 0.05%. The vector \mathbf{f}_{ext} represents the external forces. The model (see Section 2.1) considers geometrical nonlinearities and these are accounted for through the nonlinear forces \mathbf{f}_{nl} . For a given degree of freedom p , the nonlinear force is noted $f_{\text{nl},p}$, and is evaluated (using Einstein summation convention) with

$$f_{\text{nl},p} = K_{ij}^{\text{q},p} u_i u_j + K_{ijk}^{\text{c},p} u_i u_j u_k, \quad (2)$$

where u_i is the displacement of the i -th degree of freedom. The indexes i , j , and k vary within $\llbracket 1, N_{\text{dof}} \rrbracket$. The terms \mathbf{K}^{q} (third order tensor), \mathbf{K}^{c} (fourth order tensor) represent the quadratic and cubic nonlinear effects. The normal form theory is next applied and the main steps of the reduction are recalled.

First step

First are computed the eigenvectors (i.e. linear normal modes) Φ of the underlying linear conservative autonomous system of Equation (1). By substituting $\mathbf{u} = \Phi \mathbf{q}$ and projecting the system on Φ^{T} , the following modal equation is obtained for all the modes $p \in \llbracket 0, N_{\text{dof}} - 1 \rrbracket$ ¹

$$\ddot{q}_p + 2\xi_p \omega_p \dot{q}_p + \omega_p^2 q_p + g_{ij}^p q_i q_j + h_{ijk}^p q_i q_j q_k = f_{\text{ext},p}, \quad (3)$$

where ω_p and ξ_p denote the linear natural frequency and damping of the p -th mode. The indexes i , j , and k vary between $\llbracket 0, N_{\text{dof}} - 1 \rrbracket$. The terms g_{ij}^p and h_{ijk}^p are components of the projection of the tensors \mathbf{K}^{q} and \mathbf{K}^{c} on the p -th mode. The scalar $f_{\text{ext},p}$ is the projection of the external forces on the p -th mode. The system (3) is then written under a set of first order differential equations:

$$\begin{cases} \dot{q}_p = y_p \\ \dot{y}_p + 2\xi_p \omega_p y_p + \omega_p^2 q_p + g_{ij}^p q_i q_j + h_{ijk}^p q_i q_j q_k = f_{\text{ext},p} \end{cases} \quad (4)$$

¹The modes numbering starts at 0 in order for the modes of interest to be numbered 1 and 2, see Table 1.

Next, a quadratic nonlinear change of variable is applied. For each mode, the initial unknowns (\mathbf{q}, \mathbf{y}) are defined with respect to the new unknowns (\mathbf{r}, \mathbf{s}) such that:

$$q_p = r_p + a_{ij}^p r_i r_j + b_{ij}^p s_i s_j + c_{ij}^p r_i s_j \quad (5a)$$

$$y_p = s_p + \alpha_{ij}^p r_i r_j + \beta_{ij}^p s_i s_j + \gamma_{ij}^p r_i s_j \quad (5b)$$

Third step

The third step consists in evaluating the coefficients $a_{ij}^p, b_{ij}^p, c_{ij}^p, \alpha_{ij}^p, \beta_{ij}^p,$ and γ_{ij}^p of (5). For this matter, the values of q_p and y_p and their time derivative are first substituted in (4) by their new definition (5). Equations containing quadratic terms in r and s , such as for instance $r_i r_j, \dot{r}_i r_j, s_i s_j, \dot{s}_i s_j,$ etc are obtained. The terms $\dot{r}_p,$ and \dot{s}_p are then replaced by their first order expansion

$$\dot{r}_p = s_p + \mathcal{O}(r_p^2, s_p^2) \quad (6a)$$

$$\dot{s}_p = -2\xi_p \omega_p s_p - \omega_p^2 r_p + \mathcal{O}(r_p^2, s_p^2). \quad (6b)$$

In the obtained system, the monomials of each order are gathered and their coefficients must be equal to 0. This allows to evaluate the coefficients $a_{ij}^p, b_{ij}^p, c_{ij}^p, \alpha_{ij}^p, \beta_{ij}^p,$ and γ_{ij}^p . Full details on the equations and the solution can be found in [21]. In the current development, a quadratic change of variables (see Equation (5)) was performed, whereas a cubic change of variables was used in [21]. The coefficients $a_{ij}^p, b_{ij}^p, c_{ij}^p, \alpha_{ij}^p, \beta_{ij}^p,$ and γ_{ij}^p obtained are inversely proportional to the quantities $(\pm\omega_p \pm \omega_i \pm \omega_j)$ and are thus undefined when

$$\pm\omega_p \pm \omega_i \pm \omega_j \approx 0. \quad (7)$$

In Section 2.1, we developed a model such that $2\omega_1 \approx \omega_2$. Therefore, for specific values of $i, j,$ and $p,$ Equation (7) is satisfied and the associated coefficients $a_{ij}^p, b_{ij}^p, c_{ij}^p, \alpha_{ij}^p, \beta_{ij}^p,$ and γ_{ij}^p will be undefined. In this case, these coefficients are then arbitrary set to 0 (as it was similarly done in [35, 36]).

120

Fourth step

Once the coefficients are obtained, the fourth and final step consists in, once again, substituting (5) into (4) and rewriting the system of equations into a second order differential system of equations. The reduction is performed at this point in which only some modes p are kept. Let define by $\mathcal{N}_{\text{mode}}$ the set of modes kept and by $N_{\text{mode,red}}$ its size ($N_{\text{mode,red}} \leq N_{\text{dof}}$). The equation becomes

$$\ddot{r}_p + 2\xi_p \omega_p \dot{r}_p + \omega_p^2 r_p + G_{ij}^p r_i r_j + A_{ijk}^p r_i r_j r_k + B_{ijk}^p r_i \dot{r}_j \dot{r}_k + C_{ijk}^p r_i r_j \dot{r}_k = f_{\text{ext},p}, \quad p \in \mathcal{N}_{\text{mode}}, \quad (8)$$

where the indexes i, j, k take all the values in $\mathcal{N}_{\text{mode}}$. The third and fourth order tensor coefficients of Equation (8) are given by:

$$A_{ijk}^p = h_{ijk}^p + (g_{iq}^p + g_{qi}^p) a_{jk}^q \quad (9a)$$

$$B_{ijk}^p = (g_{iq}^p + g_{qi}^p) b_{jk}^q \quad (9b)$$

$$C_{ijk}^p = (g_{iq}^p + g_{qi}^p) c_{jk}^q \quad (9c)$$

$$G_{ij}^p = \begin{cases} g_{ij}^p & \text{if } (p, i, j) \text{ satisfies (7)} \\ 0 & \text{otherwise.} \end{cases} \quad (9d)$$

Notice that, in (9), the Einstein summation convention is used for the index q which varies in $\llbracket 0, N_{\text{dof}} - 1 \rrbracket$. The choice of the modes, $\mathcal{N}_{\text{mode}}$, along with the order of approximation used in the change of coordinates (see Equation (5)) define the invariant manifold on which the solution is computed [37, 35]. If a mode is not retained in the reduction, then no interaction can occur with this mode. For the test case under
 125 consideration (see Section 2.1 and 2.2), interaction is expected to occur between the first torsional mode and the second flexural mode. As a consequence, only the modes whose frequency is contained within the range $[180 \text{rad s}^{-1}, 460 \text{radian/s}]$ are kept (see Table 1 for the numerical values of ω_1 and ω_2).

For the single sector system, only two modes are kept (i.e. $\mathcal{N}_{\text{mode}} = \{1, 2\}$, $N_{\text{mode,red}} = 2$, and i, j , and k can take the value $\{1, 2\}$), and the system to solve becomes:

$$\begin{cases} \ddot{r}_1 + 2\xi_1 \omega_1 \dot{r}_1 + \omega_1^2 r_1 + \alpha r_1 r_2 + A_{ijk}^1 r_i r_j r_k + B_{ijk}^1 r_i \dot{r}_j \dot{r}_k + C_{ijk}^1 r_i r_j \dot{r}_k = 0 \\ \ddot{r}_2 + 2\xi_2 \omega_2 \dot{r}_2 + \omega_2^2 r_2 + \beta r_1 r_1 + A_{ijk}^2 r_i r_j r_k + B_{ijk}^2 r_i \dot{r}_j \dot{r}_k + C_{ijk}^2 r_i r_j \dot{r}_k = f_{\text{ext},2} \end{cases} \quad (10)$$

where $\alpha = (G_{12}^1 + G_{21}^1)$, $\beta = G_{11}^2$. The mode 2 (second bending mode) is directly excited. Due to the nonlinear change of variables and the relation between the natural frequencies given in Equation (7), the
 130 quadratic terms in (10) are limited here to $r_1 r_2$ and r_1^2 . However, the tensors of fourth order couple all the modes kept in the reduction, i.e. all possible cubic combinations between r_1, r_2 and their time derivatives exist in (10). The Einstein notation is maintained for these terms.

The normal form enables to reduce the system from N_{dof} (equal to 42 for the single sector) to $N_{\text{mode,red}}$ (reduced to 2 for the single sector) unknowns. The main limitation of the normal form theory is that, for
 135 large finite elements models, the tensors \mathbf{K}^q and \mathbf{K}^c are very big and can not be numerically stored. Their projection on the linear eigenvectors Φ may also be impossible in practice. To solve this issue, Vizzaccaro et al. [38] proposed the direct normal form approach (DNF). In our situation, the model contains few nodes and the number of sectors is kept low. Therefore, the normal form theory, presented in this Section, is applied.

However for larger structures and for a larger number of sectors (greater than five or six), the DNF may be
 140 better suited.

2.3.2. Cyclic systems

For a cyclic system, the main derivations are the same. However, some specificities need to be clarified for the first and fourth steps and these are explained next.

First step: computation of the eigenvectors

145 The eigenmodes of a cyclically symmetric system can be classified per nodal diameter ($m \in \llbracket 0, K \rrbracket$). Two kinds of modes exist: the non-degenerated modes ($m = 0$: all sectors move in unison, and $m = \frac{N}{2}$: the sectors have an alternating motion); and the degenerated modes. For degenerated modes, the natural frequencies of the system have a multiplicity of two, and two eigenvectors corresponding to traveling waves in opposite direction describe the deformed shape of the structure. The number of modes in the first step
 150 (see Equation (3)) is equal to $N \times N_{\text{dof}}$.

Fourth step: final system of equations

In the last step (see Equation (8)), there are $N \times N_{\text{mode,red}}$ unknowns to solve. The cyclic coordinates are noted $r_{m,p}$, where $m \in \llbracket 0, K \rrbracket$ is the nodal diameter and $p \in \{1, 2\}$ is the p -th mode of the m -th nodal diameter. If m is degenerated then $r_{m,p}$ it is complex and is associated to its complex conjugate with

$$r_{N-m,p} = \bar{r}_{m,p}. \quad (11)$$

For a cyclically symmetric system, Equation (10) is simply expanded on $(K + 1)$ nodal diameters and can be written

$$\begin{cases} \ddot{r}_{m,1} + 2\xi_{m,1}\omega_{m,1}\dot{r}_{m,1} + \omega_{m,1}^2 r_{m,1} + \alpha_{ij}^{m,1} r_{i,1} r_{j,2} + A_{def}^{m,1} r_d r_e r_f + B_{def}^{m,1} r_d \dot{r}_e \dot{r}_f + C_{def}^{m,1} r_d r_e \dot{r}_f = 0, & \forall m \in \llbracket 0, K \rrbracket \\ \ddot{r}_{m,2} + 2\xi_{m,2}\omega_{m,2}\dot{r}_{m,2} + \omega_{m,2}^2 r_{m,2} + \beta_{ij}^{m,2} r_{i,1} r_{j,1} + A_{def}^{m,2} r_d r_e r_f + B_{def}^{m,2} r_d \dot{r}_e \dot{r}_f + C_{def}^{m,2} r_d r_e \dot{r}_f = f_{\text{ext},m}, & \forall m \in \llbracket 0, K \rrbracket \end{cases} \quad (12)$$

where $\alpha_{ij}^{m,p} = (G_{ij}^{m,p} + G_{ji}^{m,p})$, and $\beta_{ij}^{m,p} = G_{i,j}^{m,p}$. Notice that this system is similar to (10). Indeed, the number of quadratic terms is limited (the tensor \mathbf{G} couples only specific modes that are the terms $r_{i,1} r_{j,2}$ and $r_{i,1} r_{j,1}$). The indexes i and j represent the nodal diameter numbers and vary on $\llbracket 0, N - 1 \rrbracket$ (with the
 155 property (11)). The fourth order tensors couple all the modes kept in the reduction and their time derivative, and the indexes d , e , and f may take the value of any nodal diameter for any of the modes kept.

In [20], a formula was derived analytically to predict the nodal diameters interaction. It was then used to create a reduced-order model by assuming that the vibrational response will be contained only on these

diameters. In the current paper, the reduced system (12) keeps the whole nodal diameter basis in order to recover all possible 1:2 internal resonances. However, the result of [20] on the prediction of possible modal interaction is still employed. It stipulates that, in the quadratic nonlinear forces, two nodal diameters i and j can interact through the term $r_i r_j$ and excite the m -th nodal diameter if and only if

$$i + j \equiv m \pmod{N} \quad (13)$$

If the indexes i and j do not satisfy relation (13), then the terms α_{ij}^m and β_{ij}^m are found to be equal to 0. A similar relation can be obtained for the cubic nonlinear forces.

Equation (7) expresses the frequency condition for the possible existence of a 1:2 internal resonance. Equation (13) gives the required nodal diameter condition in the case of cyclically symmetric systems. Equations (10) (for the single sector) and (12) (for the cyclic system) govern the dynamics of reduced-size models and will be solved with the numerical algorithms presented in the following section.

2.4. Numerical algorithms

Due to the periodic nature of the excitation of the system (see Equation (1)), the stationary solution is assumed to be also periodic. The Harmonic Balance Method (HBM) [39] is employed to solve the system (10) or (12). The displacement is sought after as:

$$\mathbf{r} = \mathbf{c}_0 + \frac{1}{2} \sum_{k=1}^{N_h} \left(\mathbf{c}_k e^{ik\omega t} + \bar{\mathbf{c}}_k e^{-ik\omega t} \right), \quad (14)$$

where $(\mathbf{c}_k)_{k \in \llbracket 0, N_h \rrbracket}$ are the unknown harmonic coefficients, N_h is the harmonic order, and $\bar{\bullet}$ denotes the complex conjugate. The form (14) is substituted into (10) or (12) and the nonlinear algebraic system of equations obtained after balancing the different harmonics is solved with a Newton-Raphson algorithm. To increase its rapidity, the jacobian of the system of equations is computed analytically. Moreover as needed in specific numerical tools cited below, the hessian of the system is also computed analytically. The derivations of the jacobian and hessian of the nonlinear forces are presented in the Appendix A. In the following sections, the HBM is applied with $N_h = 11$, which is sufficient to ensure convergence. The harmonic external excitation is applied on the second harmonic,

$$f_{\text{ext}}(t) = f_a \cos(2\omega t), \quad (15)$$

where f_a is a scalar value. In the numerical analysis, its value will be varied in the range $[0\text{N}, 50\text{N}]$. ω is taken around the natural linear frequency of the first torsional mode ($\omega \approx \omega_1$). As a consequence, the system

is directly excited around the second bending mode. The excitation is shifted to 2ω to recover properly the 1:2 internal resonance. In the absence of internal resonance, it is expected that the system shows a high 2ω component (motion on the second bending mode). However, if an 1:2 internal resonance occurs, the first torsional mode will respond on the first harmonic coefficient.

170 In the numerical applications, the results are presented in terms of physical coordinates. To obtain these quantities, the unknowns \mathbf{r} are found by solving (10) or (12), are then substituted in (5) (or equivalent), and are finally projected on the linear eigenvectors Φ .

175 In this paper, the HBM is coupled with a pseudo-arc length path continuation [40] and thus only a single branch is obtained by default. However, several solutions may exist at the same excitation frequency due to the nonlinear feature of the mechanical system. The methodology developed in [41] is here applied to detect and follow branch points and Neimark-Sacker points. Other methods such as the one explained in [42] could have been considered. A branch switching algorithm is also applied to follow new branches of periodic solutions emerging from previously obtained branch points. Its theory comes from Seydel [43] and Kuznetsov [44]. Details on the algorithm used can be found in Section 3.2 of [12]. Quasi-periodic solutions
180 originating from the Neimark-Sacker bifurcation points are not computed in this paper. Specific algorithms, such as the one proposed by Fontanela et al. [45] could have been employed for such analysis. The numerical solutions obtained may be stable or unstable. Only stable solutions are of interest in our study as they can be observed in practical applications. To determine the stability, the Floquet theory [46] (or see Section 3.2 in [47]) is applied.

185 The practical purpose of this paper is to explain how intrinsic nonlinear effects can be used to lower the maximal stable transversal displacement. Internal resonances are at the source of bifurcated branches with stable or unstable parts and a good prediction of all of these nonlinear effects is crucial.

The dynamics of a single sector is numerically studied next. Cyclically symmetric systems will be studied both analytically (see Section 4) and numerically (see Section 5) later.

190 3. Validation and analysis on a single sector

In this section, the reduced model of a single blade presented in Section 2.3.1 is studied with the numerical algorithms presented in Section 2.4. The last simulation of this section investigates the influence of the excitation amplitude on the possible energy transfer between modes via an internal resonance.

3.1. Analysis of the dynamic behaviour

195 In this section, we first verify the accuracy of the normal form theory and analyze the reduced-order model at high excitation amplitude (taken here as equal to 50N). Figure 4 represents the transversal displacement and the torsion angle at the tip of the blade as a function of the excitation frequency. Only the bifurcated branches stemming from the main branch are computed and represented. The Figure also represents the Neimark-Sacker points and branch points existing in all computed branches.

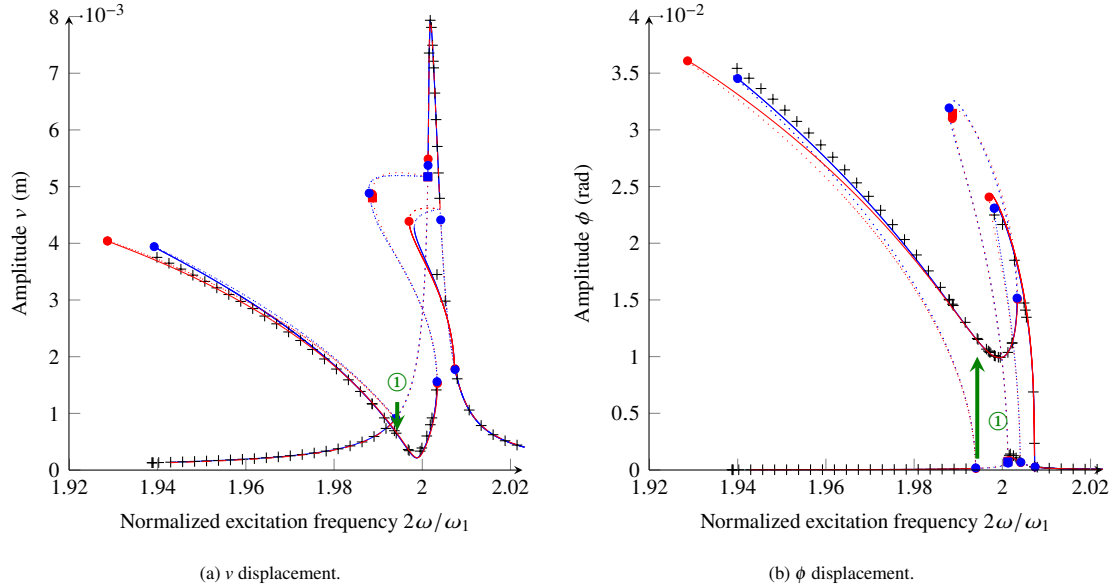


Figure 4: Frequency forced response. (—): reference solution; (—): ROM solution. Full (dotted) lines represent stable (unstable) solutions. (+): temporal integration solution. (■): Neimark-Sacker bifurcation points. (●): limit and branch points.

200 The Figure 4 shows the HBM solution of the reduced-order model (in blue) as well as the full model (in red). Numerical time integrations (black crosses) performed on the reduced-order model are also illustrated. They confirm the accuracy of the HBM on all stable branches. For an initialization on the unstable parts, the temporal integration converges toward a stable branch at the same excitation frequency (however it requires a longer time to reach this solution). Overall the results between the reduced model and the full model are very satisfactory. To increase the accuracy of the reduction, we would suggest applying the normal form theory with an higher order (see Equation (5)). Within the scope of this paper, the results are precise enough and allow to decrease the computation time from several days (taken for the reference solution with the

205

computation of Floquet stability) to a couple of minutes with the reduced-order model².

In Figure 4, a main branch as well as two bifurcated branches can be observed. To characterize the solutions and exhibit the phenomena of internal resonance, the full temporal integration corresponding to the point of calculation at normalized frequency 1.995 (which corresponds to an excitation frequency of 441.0rad s^{-1}) is presented in Figure 5. For this point of calculation, the initialization was taken equal to the unstable solution point of the HBM (on its main branch). As shown in Figure 5a, after 50s of computation, the system changes its dynamic: the amplitude of the transversal displacement decreases, and the value the torsion angle increases. Through the spectrogram (see Figure 5b), it can be observed that, initially, the frequency of the solution is at 2ω . After 50s, it becomes half the frequency of excitation. This simulation confirms the appearance of an 1:2 internal resonance: in the permanent regime, the torsional mode predominates the dynamics of the system whereas the flexural mode was directly excited.

²The simulations were run on an Intel(R) Core(TM) i7-7700 @ 3.6 GHz computer.

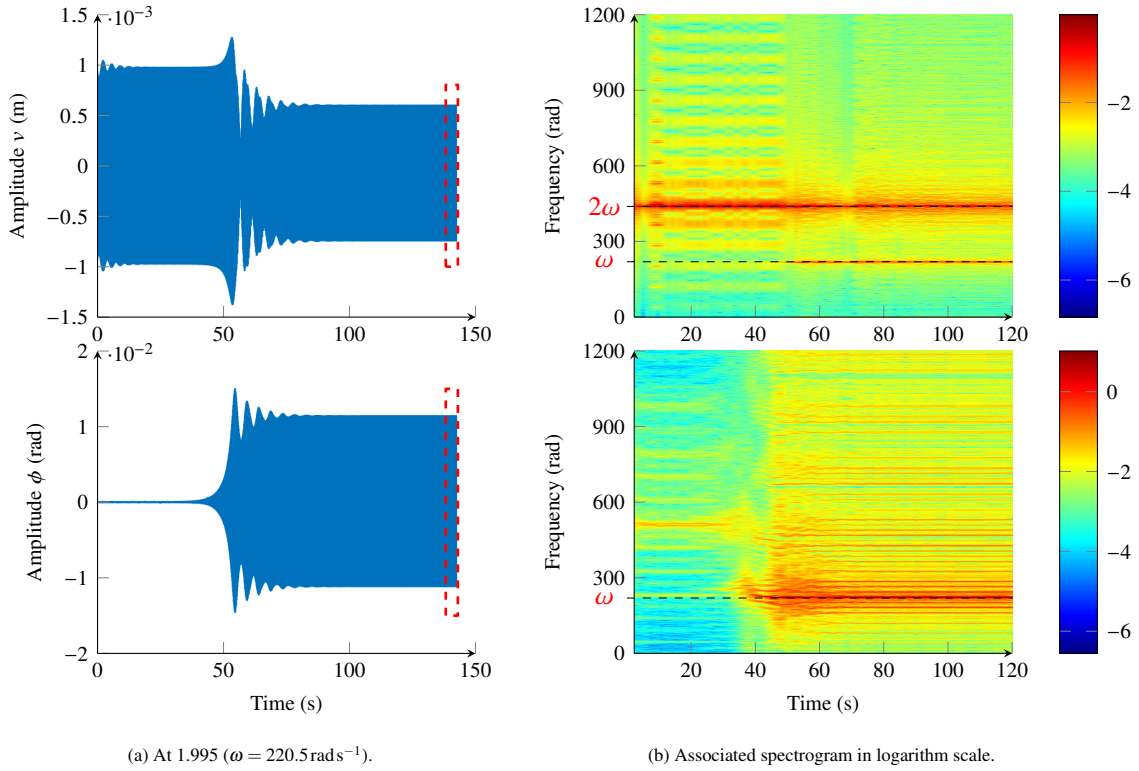


Figure 5: Temporal integration and its close-up for the green arrow of Figure 4.

In Figure 4, we observe that only some parts of the main branch are stable. The stability of this main
 220 branch is dictated by the appearance of the different bifurcated branches [47]. The purpose of the next
 section is to tune the excitation level such that the peak of the main branch becomes unstable, leading to a
 much lower value of stable transversal displacement.

For a system excited with a lower amplitude, the effect of the nonlinearities are smaller and thus the
 invariant manifold defined through the normal form theory should be more accurate. As a consequence, the
 225 following results calculated with an excitation amplitudes lower than 50N are also expected to be accurate.

3.2. Optimization of the transversal displacement

In this section, the system dynamics is analyzed for an excitation amplitude varying in the range $[0\text{N}, 50\text{N}]$.
 The purpose is to determine the range of excitation amplitude for which the internal resonance decreases the
 level of transversal displacement.

To this effect, the maximal stable transversal displacement (over the frequency range and over all branches) is recorded for each excitation level. The value used as reference corresponds to the maximal transversal displacement of the main branch. Both values are normalized with the excitation amplitude. Results are illustrated in Figure 6.

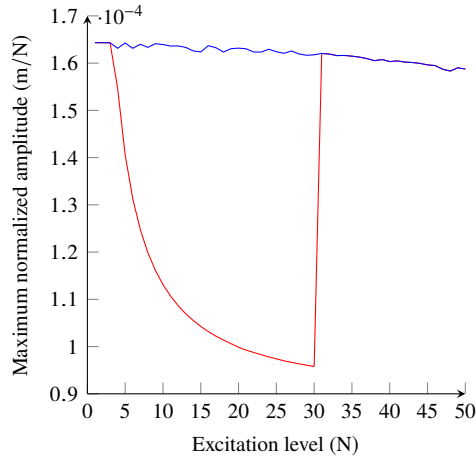


Figure 6: Normalized maximal transversal amplitude over the excitation range. (—): maximal stable displacement over all branches; (—): maximal displacement of the main branch.

In Figure 6, the blue and red curves do not coincide for an excitation amplitude within $[3\text{ N}, 30\text{ N}]$. For this range, the maximal displacement of the main branch is unstable due to presence of an internal resonances. The energy transfer occurring in the system allow to decrease the transversal displacement level. To better understand this result, the localizations of the bifurcation points for different excitation amplitudes and frequencies are computed using the method proposed in [41]. These are illustrated in Figure 7.

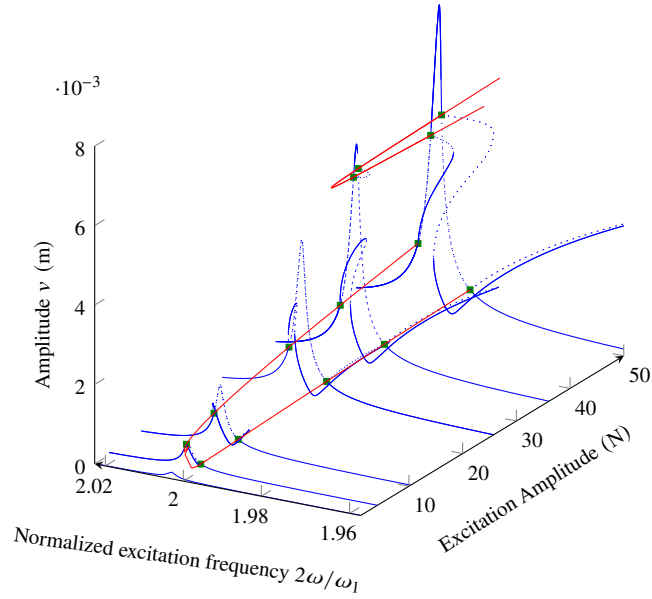


Figure 7: Tracking of the branching points. (—): localization of the branch bifurcation points. (—): frequency forced responses for different excitation amplitudes. Full (respectively dotted) lines represent stable (respectively unstable) parts of the solution. (■): branch points.

Below 3 N, Figure 7 shows that no internal resonance occurs. Between 3 N and 30 N, a single internal
 240 resonance appears. Beyond 30 N, four branch points are identified and lead to two branches with internal
 resonances. Whereas the first internal resonance leads to an unstable solution of the resonant peak of the
 second bending mode, the second internal resonance gets this peak stable again. Internal resonances may
 be interesting to exchange energy from the transversal displacement to the torsional displacement but can
 therefore be useful only for a specific range of excitation. Section 5 intends to provide similar analyses for
 245 cyclic systems. The next section first focuses on an analytical method, namely the multiple scale approach,
 to further understand the conditions of appearance of internal resonances in a cyclically symmetric system.

4. Analysis with the multiple scales method

In this section, the analytical approach of the multiple scales is employed to provide theoretical condi-
 tions to obtain 1:2 internal resonances in a system with cyclic symmetry. Notice that this work could be
 250 extended without much difficulties to other internal resonances such as 1:1, or 1:3 internal resonances.

The behaviour of a 1:2 internal resonance on a single beam has been studied extensively, for instance by Nayfeh et al. in [28] to study the 1:2 internal resonance through the multiple scales method. A second order approximation will be used in this paper to study a system with cyclic symmetry, although using an higher order [8] could also be possible.

255 4.1. Analytical developments

This sections focuses on the cyclic system presented in Section 2.2 and whose equation of motion (after reduction by the normal form approach is given in (12)). A single nodal diameter m is harmonically excited at frequency ω , with the force

$$f_{\text{ext},m} = f_A e^{i\omega t} + f_B e^{-i\omega t}, \quad (16)$$

260 where f_A , and f_B are scalar values. Let consider that the interaction between the second bending mode of the m -th nodal diameter occurs with the first torsional mode of the n -th nodal diameter (1:2 internal resonance between different diameters). The equation of motion of these two modes are

$$\begin{cases} \ddot{r}_{n,1} + 2\xi_{n,1}\omega_{n,1}\dot{r}_{n,1} + \omega_{n,1}^2 r_{n,1} + \alpha_{ij}^{n,1} r_{i,1} r_{j,2} + A_{def}^{n,1} r_d r_e r_f + B_{def}^{n,1} r_d \dot{r}_e \dot{r}_f + C_{def}^{n,1} r_d r_e \dot{r}_f = 0 \\ \ddot{r}_{m,2} + 2\xi_{m,2}\omega_{m,2}\dot{r}_{m,2} + \omega_{m,2}^2 r_{m,2} + \beta_{ij}^{m,2} r_{i,1} r_{j,1} + A_{def}^{m,2} r_d r_e r_f + B_{def}^{m,2} r_d \dot{r}_e \dot{r}_f + C_{def}^{m,2} r_d r_e \dot{r}_f = f_{\text{ext},m} \end{cases} \quad (17)$$

where the indexes i , and j may only be equal to m or n . The multiple scale approach defines different time scales $T_p = \varepsilon^p t$ of the problem, where ε is a small dimensionless parameter. Based on Table 1 and Figure 3, the following relationships between the excitation ω and modal frequencies are defined:

$$\omega = \omega_{m,2} + \varepsilon \sigma_2 \quad (18a)$$

$$2\omega_{n,1} = \omega_{m,2} + \varepsilon \sigma_1, \quad (18b)$$

The scalars σ_1 and σ_2 are two detuning parameters. Let also set

$$f_A = \varepsilon^2 f_a \quad (19a)$$

$$f_B = \varepsilon^2 f_b \quad (19b)$$

$$\xi_{n,1}\omega_{n,1} = \varepsilon \mu_{n,1} \quad (19c)$$

$$\xi_{m,2}\omega_{m,2} = \varepsilon \mu_{m,2}. \quad (19d)$$

The displacements are sought as

$$r_{n,1} = \varepsilon r_{n,11}(T_0, T_1) + \varepsilon^2 r_{n,12}(T_0, T_1) \quad (20a)$$

$$r_{m,2} = \varepsilon r_{m,21}(T_0, T_1) + \varepsilon^2 r_{m,22}(T_0, T_1) \quad (20b)$$

Substituting these equations into (17) gives a system of equations for the different orders of ε . The first order gives

$$\begin{cases} D_0^2 r_{n,11} + \omega_{n,1}^2 r_{n,11} = 0 \\ D_0^2 r_{m,21} + \omega_{m,2}^2 r_{m,21} = 0 \end{cases} \quad (21)$$

where $D_p = \frac{\partial}{\partial T_p}$. For the order ε^2 , one has:

$$\begin{cases} D_0^2 r_{n,12} + \omega_{n,1}^2 r_{n,12} = -2D_0 D_1 r_{n,11} - 2\mu_1 D_0 r_{n,11} - \alpha_{ij}^{n,1} r_{i,11} r_{j,21} \\ D_0^2 r_{m,22} + \omega_{m,2}^2 r_{m,22} = -2D_0 D_1 r_{m,21} - 2\mu_2 D_0 r_{m,21} - \beta_{ij}^{m,2} r_{i,11} r_{j,11} + f_{\text{ext},m} \end{cases} \quad (22)$$

Solving (21) gives

$$r_{n,11} = \begin{cases} A_n(T_1) e^{i\omega_{n,1} T_0} + B_n(T_1) e^{-i\omega_{n,1} T_0}, & \text{if } n \text{ is degenerated} \\ A_n(T_1) e^{i\omega_{n,1} T_0} + c.c., & \text{if } n \text{ is non degenerated} \end{cases} \quad (23)$$

A similar solution is obtained for $r_{m,2,1}$ with the unknowns A_m and B_m . Four cases are then possible depending of the value of n and m : they either correspond to two degenerated nodal diameters, two non-degenerated ones, or there is one of each. Only the first case is fully treated in the following demonstration, but results of all cases are given at the end of this section.

Let consider both nodal diameters degenerated, one must then account for the coupling with their associated complex conjugate terms (see Equation (11)) in the nonlinear forces of (22). Therefore, the quadratic terms of (22) can be developed to

$$\begin{aligned} \alpha_{ij}^{n,1} r_{i,11} r_{j,21} &= \alpha_{nm}^{n,1} (r_{n,11} r_{m,21}) + \alpha_{(N-n)m}^{n,1} (r_{N-n,11} r_{m,21}) \\ &\quad + \alpha_{n(N-m)}^{n,1} (r_{n,11} r_{N-m,21}) + \alpha_{(N-n)(N-m)}^{n,1} (r_{N-n,11} r_{N-m,21}) \end{aligned} \quad (24)$$

and

$$\begin{aligned} \beta_{ij}^{m,2} r_{i,11} r_{i,11} &= \beta_{mm}^{n,1} (r_{n,11} r_{n,11}) + \left(\beta_{(N-n)n}^{n,1} + \beta_{n(N-n)}^{n,1} \right) (r_{N-n,11} r_{n,11}) \\ &\quad + \beta_{(N-n)(N-m)}^{n,1} (r_{N-n,11} r_{N-n,11}) \end{aligned} \quad (25)$$

Equations (24) and (25) are substituted in (22) to derive the following solvability conditions:

$$\begin{cases} -2i\omega_1 (A'_n + \mu_1 A_n) - \left(\alpha_{nm}^{n,1} A_m B_n + \alpha_{(N-n)m}^{n,1} A_m \bar{A}_n + \alpha_{n(N-m)}^{n,1} \bar{B}_m B_n + \alpha_{(N-n)(N-m)}^{n,1} \bar{B}_m \bar{A}_n \right) e^{-i\sigma_1 T_1} = 0 \\ -2i\omega_2 (A'_m + \mu_2 A_m) - \left(\beta_{nn}^{m,2} A_n^2 + \left(\beta_{(N-n)n}^{n,1} + \beta_{n(N-n)}^{n,1} \right) A_n \bar{B}_n + \beta_{(N-n)(N-m)}^{n,1} \bar{B}_n^2 \right) e^{i\sigma_1 T_1} + f_A e^{i\sigma_2 T_1} = 0 \\ 2i\omega_1 (B'_n + \mu_1 B_n) - \left(\alpha_{nm}^{n,1} B_m A_n + \alpha_{(N-n)m}^{n,1} B_m \bar{B}_n + \alpha_{n(N-m)}^{n,1} \bar{A}_m A_n + \alpha_{(N-n)(N-m)}^{n,1} \bar{A}_m \bar{B}_n \right) e^{-i\sigma_1 T_1} = 0 \\ 2i\omega_2 (B'_m + \mu_2 B_m) - \left(\beta_{nn}^{m,2} B_n^2 + \left(\beta_{(N-n)n}^{n,1} + \beta_{n(N-n)}^{n,1} \right) B_n \bar{A}_n + \beta_{(N-n)(N-m)}^{n,1} \bar{A}_n^2 \right) e^{i\sigma_1 T_1} + f_B e^{-i\sigma_2 T_1} = 0 \end{cases} \quad (26)$$

This set of equation is nearly identical to the solvability condition obtained when the multiple scale approach is applied on a single sector (see for instance Equation (58) in [12] or Equation (9) in [28]). The main difference is that the coefficients $\alpha^{n,1}$ and $\beta^{m,2}$ may be equal to 0 in our situation. This is due to the condition of coupling between nodal diameters [20] and recalled in Equation (13). In Equation (26), the term $\alpha_{nm}^{n,1} A_m B_n$ exist if and only if the n -th and m -th nodal diameters can get coupled to excite the n -th nodal diameter. Similarly the term $\beta_{nn}^{m,2} A_n^2$ exists if the n -th nodal diameter excites the m -th nodal diameter through a quadratic nonlinearity, and so on. Therefore diameters m and n can get coupled only if

$$\pm(m+n) \equiv n \pmod{N} \quad (27a)$$

$$\pm(m-n) \equiv n \pmod{N} \quad (27b)$$

$$\pm(m+n) \equiv N-n \pmod{N} \quad (27c)$$

$$\pm(m-n) \equiv N-n \pmod{N} \quad (27d)$$

Some of these conditions are redundant and this set of condition gets simplified into

$$m \equiv 0 \pmod{N} \quad (28a)$$

$$(m-2n) \equiv 0 \pmod{N} \quad (28b)$$

$$(m+2n) \equiv 0 \pmod{N} \quad (28c)$$

As m corresponds to a degenerated nodal diameter, only the last two conditions (28b) and (28c) need to be studied.

4.2. Results and discussion

Table 2 summarizes the different conditions for all the possible combinations of nodal diameter m and n . If one of these equations is satisfied, then internal resonance may occur between the m -th nodal diameter and

the n -th nodal diameter. Table 2 gives the nodal diameters condition for the existence of internal resonance, but the associated frequency of the modes must also be quasi-commensurable (and verify Equation (18b)).

	m degenerated	m non-degenerated
	$(m - 2n) \equiv 0 \pmod{N}$	$m \equiv 0 \pmod{N}$
n degenerated	$(m + 2n) \equiv 0 \pmod{N}$	$(m - 2n) \equiv 0 \pmod{N}$ $(m + 2n) \equiv 0 \pmod{N}$
n non-degenerated	$(m - 2n) \equiv 0 \pmod{N}$ $(m + 2n) \equiv 0 \pmod{N}$	$(m - 2n) \equiv 0 \pmod{N}$

Table 2: Conditions to obtain internal resonances for cyclic systems.

Very interesting results can be deduced from the conditions given in Table 2. For instance,

- if the 0-th nodal diameter is excited ($m = 0$ is non-degenerated) then internal resonances may occur with any other nodal diameter.
- if m is both degenerated and odd, and if N is even then no internal resonance occur at all.
- if $m = \frac{N}{2}$ then an internal resonance may occur with $n = \frac{N}{4}$ if N is divisible by 4.

These analytical results are very interesting to design cyclic symmetric structure. It gives indeed the nodal diameters for which internal resonance may occur and thus provides insight on which energy transfer is possible to guide the vibrational energy of the system. In the following section, numerical simulations will be performed to analyze internal resonances on the cyclic systems so as to verify these analytical results.

These simulations go beyond the analysis of the multiple scales as high excitation will be considered.

A possible extension of this work would be to study cascades of internal resonances as proposed in [9].

5. Numerical analysis for cyclic systems

In Section 3, relevant numerical algorithms were used to analyze the behaviour of a single sector. These algorithms are now applied on the cyclic systems. The analytical results of Section 4.1 provide theoretical conditions for the existence of internal resonance. In this section, those are verified numerically for different

numbers of sectors. Similarly to what was performed in Section 3.2, investigations are then made to determine the range of excitation amplitude for which the internal resonances allow to decrease the transversal displacement.

5.1. Detailed analysis of the dynamic behaviour for $N = 2$, $m = 0$

300 As it was performed previously in Section 3.1, the system is first analyzed for a specific excitation level before optimizing the transversal displacement reduction over a range of excitation amplitude. Let consider the cyclic system of Figure 2 with only two sectors ($N = 2$) excited with an engine order equal to 0, i.e. vibration is in unison, and an amplitude of 50N. The transversal displacement and torsion angle at the tip of the first sector obtained with the HBM on the reduced system are illustrated in Figure 8 (the second sector presents identical results and is thus not represented). Figure 8 also shows numerical temporal integrations
 305 presents identical results and is thus not represented). Figure 8 also shows numerical temporal integrations initiated on the main branch found by the HBM.

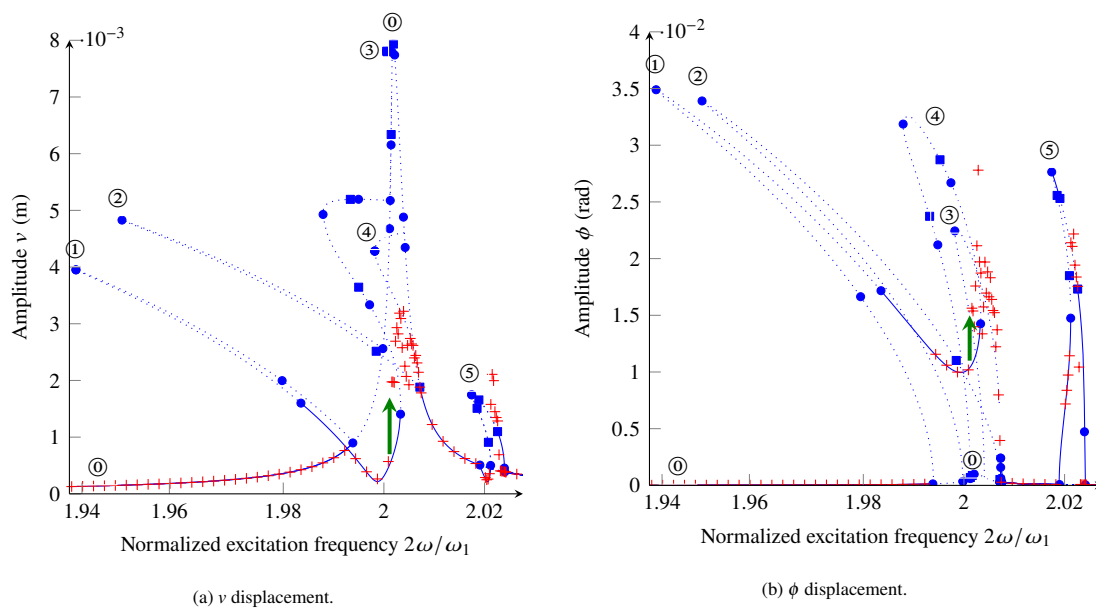


Figure 8: Frequency forced response. (—): HBM solution. Full (dotted) lines represent stable (unstable) solutions. (+): temporal integration solution. (■): Neimark-Sacker bifurcation points. (●): limit and branch points. [→]: position of future temporal integration visualization (see Figure 11).

In Figure 8, one can identify the main branch (numbered 0) as well as five bifurcated branches (numbered from 1 to 5). As $N = 2$, the solution can be decomposed on the non-degenerated nodal diameters $n = 0$, and

$n = 1$, whose HBM expansion follow Equation (14). Further analyses of these solutions are given in Figure 9 that depicts the modulus of each Fourier coefficient $(c_{k,n})_{k \in \llbracket 0,2 \rrbracket}$ of the two different nodal diameters n ($n = 0$ or $n = 1$) at the peak of each branch illustrated in Figure 8. For better readability, only the first and second harmonics are represented (the other harmonics have negligible values). In Figures 9b (branch 1), and 9e (branch 4), we observe that the torsional displacement is dominant and that it is expressed mainly by the first harmonic of the 0-th nodal diameter. These branches therefore correspond to 1:2 internal resonances within modes of the 0-th nodal diameter. The other bifurcated branches (2, 3, and 5) correspond to 1:2 internal resonances between the 0-th and 1-st nodal diameters. The multiple scales analysis predicted these interactions (see the last column of Table 2).

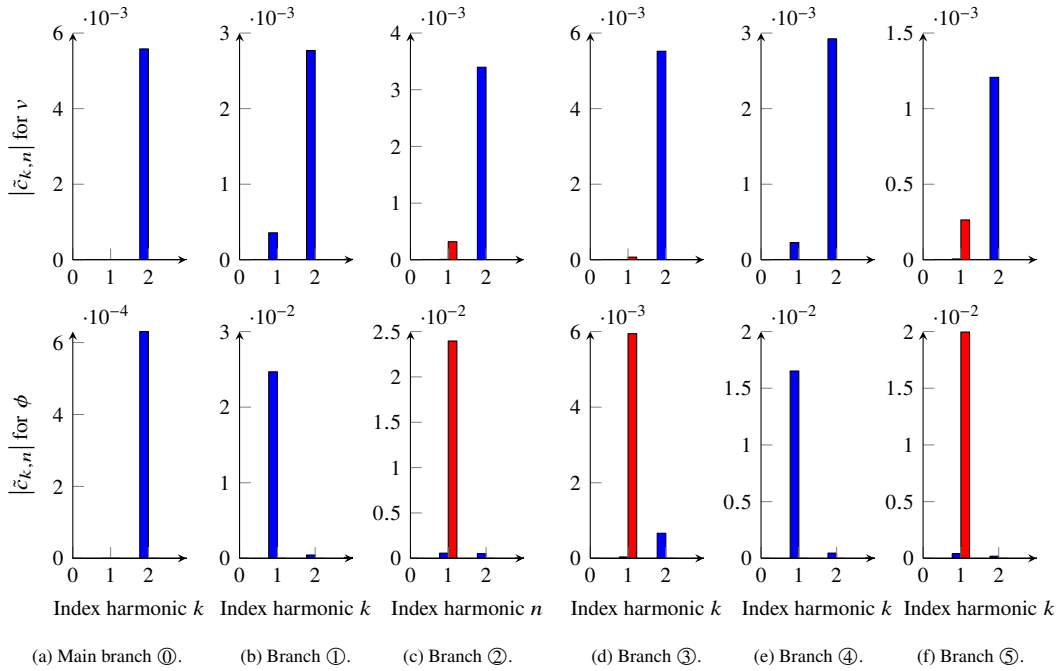


Figure 9: Harmonic content of the nodal diameters for the different branches of Figure 8. These values are given at the peak of each bifurcated branch. Blue bars (—) correspond to the 0-th nodal diameter and red bars (—) to the first nodal diameter.

Although five branches of solutions are observed for the amplitude excitation of 50N, it is difficult to know, a priori, the level of amplitude needed for these branches to arise. If one focuses on the transversal displacement, the localization of the five branch points (numbered from 1 to 5) are depicted in Figure 10 as a function of both excitation amplitude and frequency. Those were obtained following the algorithm explained in [41]. An additional bifurcated branch (which in our cases corresponds to a new internal resonance

phenomenon) appears when the excitation amplitude exceeds the following values: 2.8N, 14.5N, 24.7N, 30.5N, and 49N. This kind of analysis would have been complicated to obtain with an analytical approach such as the multiple scales analysis. Therefore, these algorithms provide interesting complementary results to Section 4.1 and give further insights on the range of excitation on which the exchange of energy may occur.

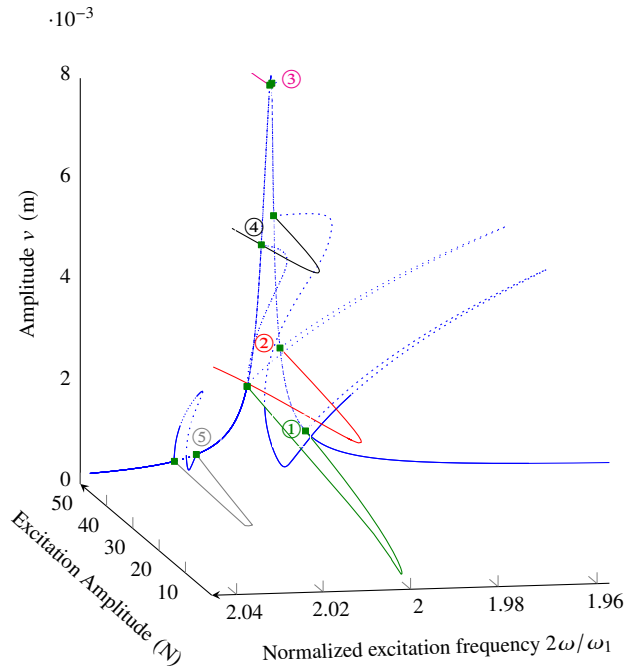


Figure 10: Tracking of the branch points. (—): frequency forced response at 50N excitation amplitude. Full (respectively dotted) lines represent stable (respectively unstable) parts of the solution. Other colored curves represent the branch points localization as a function of excitation frequency and amplitude. (■): branch points at 50N

The overall stability of the system with cyclic symmetry (see Figure 8) is different from the single sector case (see Figure 4). This is due to the additional bifurcated branches and Neimark-Sacker bifurcated points. Moreover, stable solutions that are not periodic exist on some excitation frequency ranges and are retrieved by the numerical time integration only. These are depicted in Figure 8. When initialized around the stable HBM solution, numerical time integration converges toward this periodic solution. However when initialized on an unstable solution, it converges toward a cluster of points. To analyze these solutions, the displacement and torsion angle calculated by time integration for a specific excitation frequency (shown with the green

335 arrow in Figure 8) are presented in Figure 11 as a function of time:

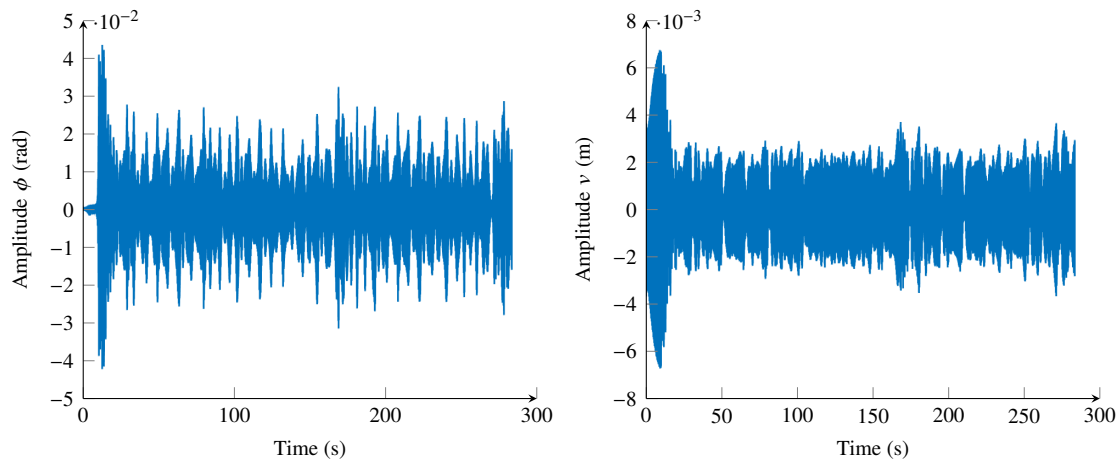


Figure 11: Temporal integration at the green arrow of Figure 8.

The regime illustrated in Figure 11 is chaotic and this shows that cyclic systems seem to exhibit a more complex behaviour than classical systems without symmetry. Further analyses of this regimes can be found in the Chapter 5 of [47] or in [48] which also handles system with symmetry.

5.2. Summary of the results

340 In this section, the systems built for $N \in \llbracket 2, 5 \rrbracket$ are studied numerically and with the multiple scales approach. For each case, one looks for the possible apparition of an internal resonance between the second bending mode of nodal diameter m ($m \in \llbracket 0, K \rrbracket$), mode directly excited by the external force, and the first torsional mode of the nodal diameter n .

345 Tables 3 and 4 summarize the results for different N and m . The case $N = 0$ and $m = 2$ was already presented in Section 5.1. The numerical results that correspond to other cases are not detailed here for brevity. In these Tables 3 and 4, for the multiple scales analysis (MSA), \checkmark indicates that internal resonances may occur and \times indicates when no interaction is expected. For the numerical analysis (NA): the lowest value of excitation amplitude for which the internal resonance appears is given; and \times indicates that no internal resonance is obtained on the studied excitation range.

N	2				3			
m	0		1		0		1	
n	0	1	0	1	0	1	0	1
MSA	✓	✓	✗	✗	✓	✓	✗	✓
NA (inN)	3	15	✗	✗	3	11	✗	25

Table 3: Occurrence of internal resonance for $N \in \{2, 3\}$.

N	4									5								
m	0			1			2			0			1			2		
n	0	1	2	0	1	2	0	1	2	0	1	2	0	1	2	0	1	2
MSA	✓	✓	✓	✗	✗	✗	✗	✓	✗	✓	✓	✓	✗	✗	✓	✗	✓	✗
NA (inN)	3	8	15	✗	✗	✗	✗	42	✗	3	5	13	✗	✗	2	✗	41	✗

Table 4: Occurrence of internal resonance for $N \in \{4, 5\}$.

350 As one can be observed in these Tables 3 and 4, there is a perfect correlation between the theoretical results of Section 4.1 and the numerical results: if the multiple scales analysis expects the presence of an internal resonance, it is also simulated numerically. On the other hand, if no internal resonance is predicted analytically, then it is also not observed in the numerical analysis, or at least not with an excitation up to 50N.

355 5.3. Optimization of the transversal displacement

In this section, the internal resonances are employed to decrease the transversal displacement of the cyclic structure. The maximal stable transversal displacement over the excitation frequency range is recorded as a function of the excitation amplitude. This leads to the prediction of the range of amplitude excitation for which the transfer of energy is efficient.

360 To have such an energy exchange, the theoretical conditions of Section 4.1 (also summarized in Tables 3 and 4) must be verified. Here two cases are considered $\{N = 2, m = 0\}$, and $\{N = 5, m = 1\}$. The associated results are presented in Figures 12a and 12b.

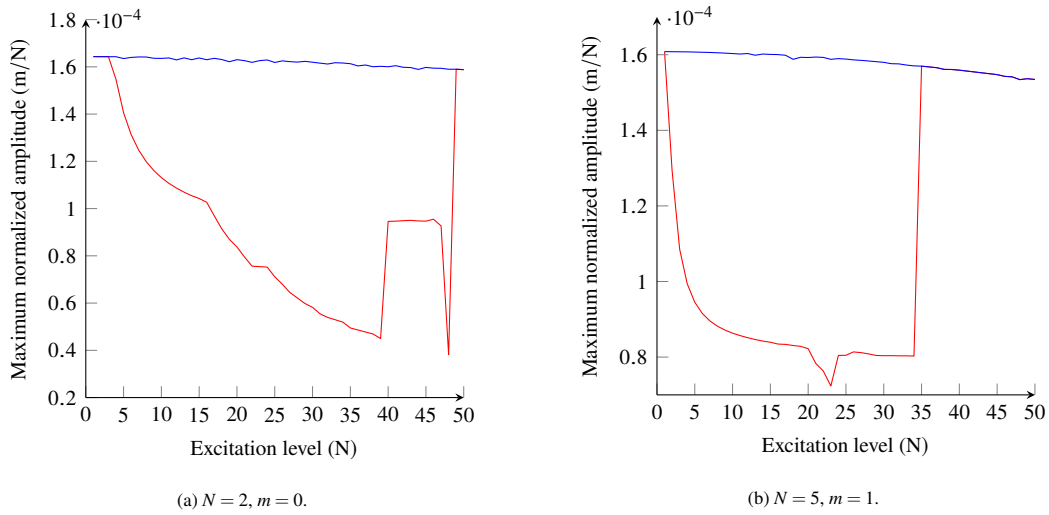


Figure 12: Normalized maximal transversal amplitude over the excitation range. (—): maximal stable displacement over all branches; (—): maximal displacement of the main branch.

In both cases, the presence of an internal resonance allows to decrease the transversal displacement over a wide range of excitation amplitude. These results are similar to the ones illustrated in Figure 6. However, they are not as smooth as the single sector case due to the existence of multiple internal resonances occurring in the systems influencing their stability.

The first "jump" of the normalized displacement amplitude is located for $N = 2$ and $m = 0$ at 40N. It occurs due to the creation of a new bifurcated branch that originates from another already existing bifurcated branch. This phenomenon is illustrated in Figure 13. The stable part observed on the box inset remains stable until two bifurcated branches merge. This is represented in Figure 14 and explains the second jump of Figure 12a occurring at 48N. The peak of the main branch then gets stable at 49N due to a new bifurcated branch (see the number 3 circled in Figure 10) leading to the final jump of Figure 12a.

In both cases, the internal resonances are efficient over a large amplitude range and decrease the normalized displacement. It is however difficult to generalize these results. For example, in the case $N = 5$, $m = 2$ (not illustrated here), the internal resonance with the first nodal diameter (that is, in this case, the only interaction observed) occurs at 41N and thus the transfer of energy is not as efficient as cases illustrated in Figures 12a and 12b.

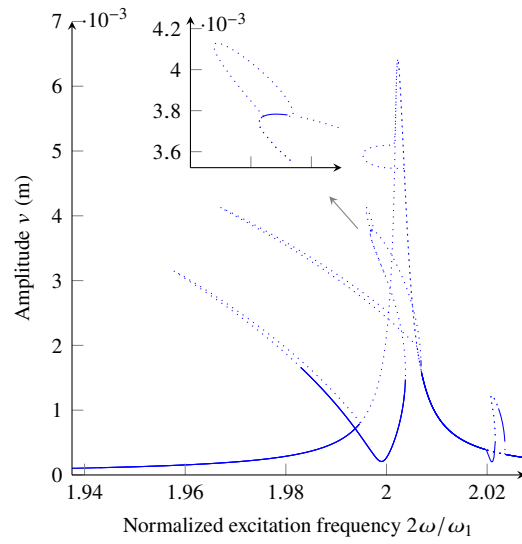


Figure 13: Frequency forced response for $N = 2$, $m = 0$, and $40N$. (—): ROM solution. Full (dotted) lines represent stable (unstable) solutions. The box inset represents the stable branch leading to the jump of Figure 12a.

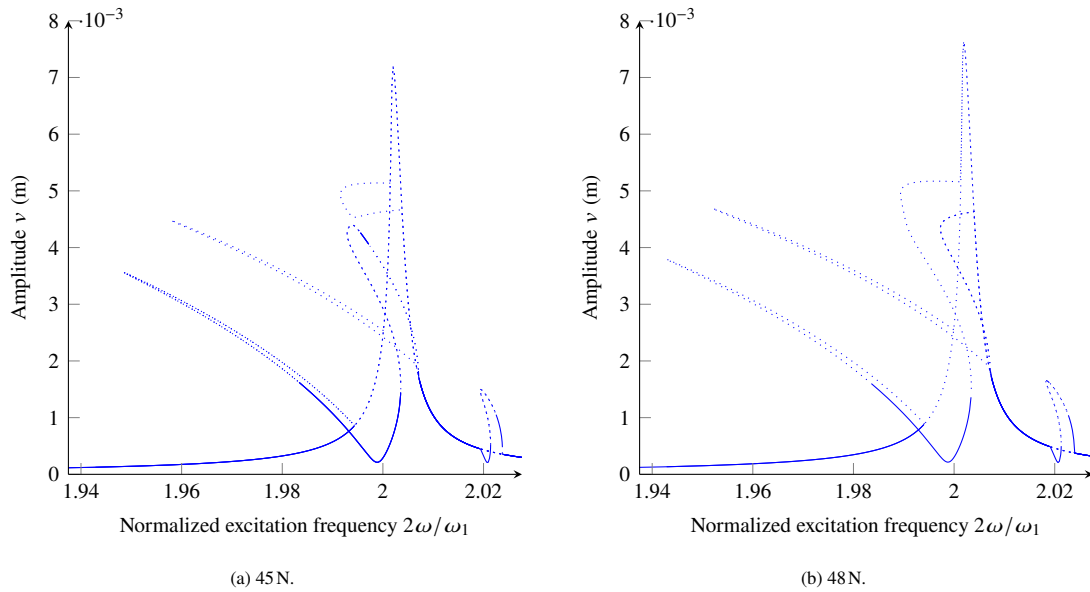


Figure 14: Frequency forced response for $N = 2$, $m = 0$. Illustration of the merge when the excitation amplitude increases. (—): ROM solution.

6. Application of global vibration mitigation exploiting internal resonances

Section 4.1 gave some conditions on the nodal diameters to obtain potential internal resonances. The
380 previous section verified these results through numerical simulations. The purpose of this Section is now to
exploit these internal resonances to transfer the energy of a mode to another one, that must be more damped,
in order to reduce the overall vibrational energy of the system. To model such effect, the damping matrix of
the system is modified such that the modal damping of the first torsional mode is increased to

$$\xi_1 = 0.05\% \times \zeta \quad (29)$$

where ζ is a scalar value which will take the value $\{1, 1.5, 3\}$. In practice, we could achieve this by coating
385 the structure with a specific material.

As previously demonstrated in Sections 3.2 and 5.3, the internal resonance leads to a decrease in the
transversal displacement and an increase in the torsional displacement. As energy transfer between modes
occurs with internal resonances, increasing the damping of the first mode should allow to decrease both the
transversal and torsional displacement of the bifurcated branch.

390 As a practical example, let consider the system with $N = 5$, excited with a traveling wave excitation with
 $m = 1$. The excitation amplitude is taken to vary within the range $[1\text{N}, 50\text{N}]$. The normalized maximum
stable transversal (respectively torsional) displacement over the excitation frequency range is illustrated in
Figure 15a (respectively Figure 15b).

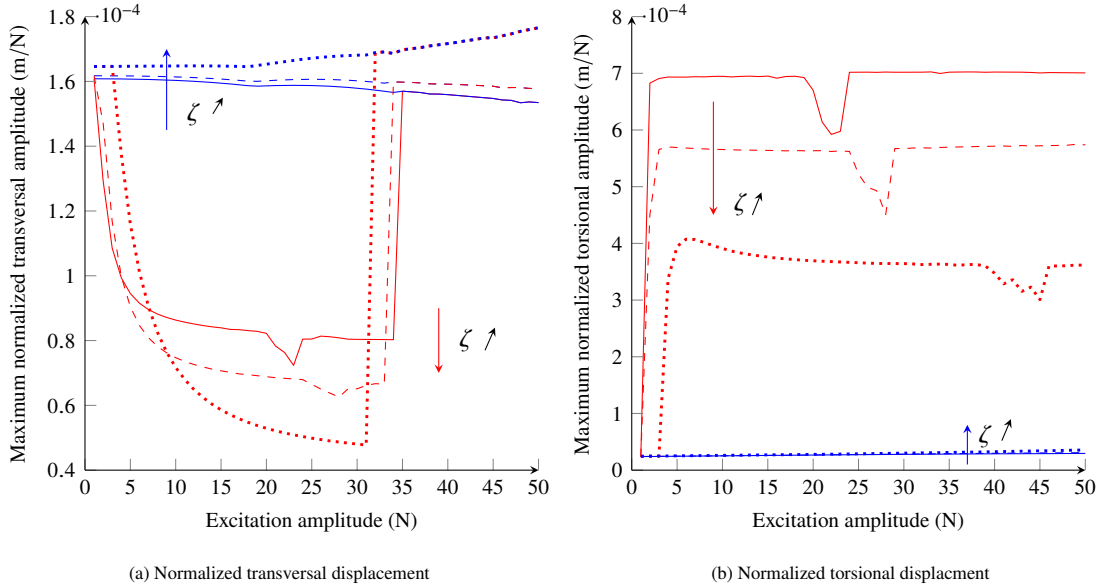


Figure 15: Normalized maximum displacements $N = 5$, $m = 1$. (—): $\zeta = 1$, (- -): $\zeta = 1.5$, and (····): $\zeta = 3$. Blues curves correspond to maximal displacements of the main branch. Red curves correspond to stable displacements over all branches.

Figure 15 shows that the energy inserted in the system via the external excitation on the second mode is properly transferred to the first one and then dissipated through damping. It also shows that as ζ increases, the effective range of excitation amplitude (for which the internal resonance occurs) is getting narrower.

This practical application demonstrated that internal resonances may be used to mitigate the vibration of mechanical systems, and enable to control the vibration level of the structures.

7. Conclusion

In this work, theoretical conditions on nodal diameters were derived in order to obtain 1:2 internal resonances in cyclic symmetric systems. These conditions were verified numerically by using a simplified yet realistic nonlinear blade model, reduced by the normal form theory, that was later extended to a cyclic system. The second bending mode of the structure was excited and energy transfer toward the first torsional mode was illustrated. The numerical solution of the system with the HBM and branch switching algorithms was shown to be in perfect agreement with the theoretical conditions for the large range of amplitude excitation studied in this paper. Further numerical investigations were conducted to better understand the nonlinear dynamics of the system and to determine the range of amplitude excitation which minimizes the transversal

displacement of the system. A short application was also proposed to show that for a set of appropriate parameters, one can decrease the global vibration of the system by exploiting the internal resonance effects.

410 Although this paper studies the specific 1:2 internal resonance, similar analyses could be performed for any internal resonances.

Combining this work with [12] (in which a geometrical parameter controlling the internal resonance was identified) would help design the blades and predict the range of excitation where the displacement is at its lowest. This work is expected to find several applications. For instance, in the field of aeronautics, designers
415 may use or avoid these internal resonances to better design engines.

Acknowledgements

The authors would like to acknowledge the financial support of Safran Helicopter Engines.

Appendix

A. Computation of the Jacobian of the systems

In order to compute the solution of the systems (12), and (10), it is necessary to provide their jacobian. The paper of [41] provides all the useful information except for the nonlinear forces. With the model reduced by the normal form theory, the following expression gives the nonlinear force for a control coordinate p

$$f_{\text{nl},p} = G_{ij}^p r_i r_j + A_{ijk}^p r_i r_j r_k + B_{ijk}^p r_i \dot{r}_j \dot{r}_k + C_{ijk}^p r_i r_j \dot{r}_k. \quad (\text{A.1})$$

The system of equations is solved through the HBM, and thus the nonlinear force (A.1) must be computed in the frequency domain. The AFT procedure [49] is used for this matter. To switch from the time domain to the frequency domain, we define the Discrete Fourier Transform, matrix \mathbf{D} ,

$$\mathbf{c} = \mathbf{D}\mathbf{r}, \quad (\text{A.2})$$

where \mathbf{r} is the displacement vector for a discretized period of time (n_{it} instants are computed), and \mathbf{c} its Fourier's coefficients. To switch from the frequency domain to the time domain, we define the Inverse Discret Fourier transform, matrix \mathbf{D}^* ,

$$\mathbf{r} = \mathbf{D}^*\mathbf{c}. \quad (\text{A.3})$$

420 A. *Computation of the jacobian : first order derivatives*

The derivative of the nonlinear forces in the frequency domain, \mathbf{F}_{nl} , with respect to \mathbf{c} , are first computed:

$$\begin{aligned} \frac{\partial \mathbf{F}_{nl}}{\partial \mathbf{c}} &= \frac{\partial \mathbf{F}_{nl}}{\partial \mathbf{f}_{nl}} \frac{\partial \mathbf{f}_{nl}}{\partial \mathbf{c}} \\ &= \mathbf{D} \left(\frac{\partial \mathbf{f}_{nl}}{\partial \mathbf{r}} \frac{\partial \mathbf{r}}{\partial \mathbf{c}} + \frac{\partial \mathbf{f}_{nl}}{\partial \dot{\mathbf{r}}} \frac{\partial \dot{\mathbf{r}}}{\partial \mathbf{c}} \right) \\ &= \mathbf{D} \left(\frac{\partial \mathbf{f}_{nl}}{\partial \mathbf{r}} \mathbf{D}^* + \frac{\partial \mathbf{f}_{nl}}{\partial \dot{\mathbf{r}}} \omega \nabla \mathbf{D}^* \right). \end{aligned} \quad (\text{A.4})$$

For a discretized instant, and two different modes p and q , one gets

$$\frac{f_{nl,p}}{r_q} = \left(G_{qj}^p + G_{jq}^p \right) r_j + \left(A_{qjk}^p + A_{jqk}^p + A_{jkq}^p \right) r_j r_k + B_{qjk}^p r_i \dot{r}_j \dot{r}_k + \left(C_{qjk}^p C_{jqk}^p + \right) r_j \dot{r}_k \quad (\text{A.5a})$$

$$\frac{f_{nl,p}}{\dot{r}_q} = \left(B_{iqj}^p + B_{ijq}^p \right) r_i \dot{r}_j + C_{ijq}^p r_j r_i r_j \quad (\text{A.5b})$$

Similarly for the derivative with respect to ω , one gets:

$$\frac{\partial \mathbf{F}_{nl}}{\partial \omega} = \mathbf{D} \left(\frac{\partial \mathbf{f}_{nl}}{\partial \dot{\mathbf{r}}} \nabla \mathbf{D}^* \mathbf{c} \right). \quad (\text{A.6})$$

B. *Computation of the Hessian: second order derivatives*

To localize the bifurcation points and to compute the others branches of the systems, it is necessary to evaluate, among other things, the derivatives of $\frac{\partial \mathbf{F}_{nl}}{\partial \mathbf{c}} \phi_1$ with respect to \mathbf{c} , and ω , where ϕ_1 is a vector. The other derivatives that need to be computed follow similar derivations and are thus not developed here for brevity.

$$\begin{aligned} \frac{\partial}{\partial \mathbf{c}} \left(\frac{\partial \mathbf{F}_{nl}}{\partial \mathbf{c}} \phi_1 \right) &= \frac{\partial}{\partial \mathbf{c}} \left(\mathbf{D} \frac{\partial \mathbf{f}_{nl}}{\partial \mathbf{r}} \mathbf{D}^* \phi_1 + \mathbf{D} \frac{\partial \mathbf{f}_{nl}}{\partial \dot{\mathbf{r}}} \omega \nabla \mathbf{D}^* \phi_1 \right) \\ &= \frac{\partial}{\partial \mathbf{c}} \left(\mathbf{D} \frac{\partial \mathbf{f}_{nl}}{\partial \mathbf{r}} \phi_{1t} + \mathbf{D} \frac{\partial \mathbf{f}_{nl}}{\partial \dot{\mathbf{r}}} \dot{\phi}_{1t} \right) \end{aligned} \quad (\text{A.7})$$

where ϕ_{1t} and $\dot{\phi}_{1t}$ represent the temporal displacement and velocity of the frequency vector ϕ_1 . Additional derivations give

$$\begin{aligned} \frac{\partial}{\partial \mathbf{c}} \left(\frac{\partial \mathbf{F}_{nl}}{\partial \mathbf{c}} \phi_1 \right) &= \mathbf{D} \frac{\partial}{\partial \mathbf{r}} \left(\frac{\partial \mathbf{f}_{nl}}{\partial \mathbf{r}} \phi_{1t} + \frac{\partial \mathbf{f}_{nl}}{\partial \dot{\mathbf{r}}} \dot{\phi}_{1t} \right) \mathbf{D}^* \\ &+ \mathbf{D} \frac{\partial}{\partial \dot{\mathbf{r}}} \left(\frac{\partial \mathbf{f}_{nl}}{\partial \mathbf{r}} \phi_{1t} + \frac{\partial \mathbf{f}_{nl}}{\partial \dot{\mathbf{r}}} \dot{\phi}_{1t} \right) \omega \nabla \mathbf{D}^* \end{aligned} \quad (\text{A.8})$$

It then remains to compute the terms $\frac{\partial}{\partial \mathbf{r}} \left(\frac{\partial \mathbf{f}_{nl}}{\partial \mathbf{r}} \phi_{1t} \right)$, $\frac{\partial}{\partial \mathbf{r}} \left(\frac{\partial \mathbf{f}_{nl}}{\partial \dot{\mathbf{r}}} \phi_{1t} \right)$, $\frac{\partial}{\partial \dot{\mathbf{r}}} \left(\frac{\partial \mathbf{f}_{nl}}{\partial \mathbf{r}} \phi_{1t} \right)$, and $\frac{\partial}{\partial \dot{\mathbf{r}}} \left(\frac{\partial \mathbf{f}_{nl}}{\partial \dot{\mathbf{r}}} \phi_{1t} \right)$. For a discretized instant, and two modes p and q , one gets:

$$\begin{aligned} \frac{\partial}{\partial r_q} \left(\frac{\partial f_{nl,p}}{\partial r_i} \phi_{1t,i} \right) &= \left(A_{kqi}^p + A_{kqi}^p + A_{ikq}^p + A_{qki}^p + A_{iqk}^p + A_{qik}^p \right) r_k \phi_{1t,i} \\ &+ \left(C_{iqk}^p + C_{qik}^p \right) \dot{r}_k \phi_{1t,i} \end{aligned}, \quad (\text{A.9})$$

$$\frac{\partial}{\partial r_q} \left(\frac{\partial f_{nl,p}}{\partial \dot{r}_i} \phi_{1t,i} \right) = \left(B_{qik}^p + B_{qki}^p \right) \dot{r}_k \phi_{1t,i} + \left(C_{qki}^p + C_{kqi}^p \right) r_k \phi_{1t,i}, \quad (\text{A.10})$$

$$\frac{\partial}{\partial \dot{r}_q} \left(\frac{\partial f_{nl,p}}{\partial \dot{r}_i} \phi_{1t,i} \right) = \left(B_{iqk}^p + B_{ikq}^p \right) \dot{r}_k \phi_{1t,i} + \left(C_{ikq}^p + C_{kqi}^p \right) r_k \phi_{1t,i}, \quad (\text{A.11})$$

and

$$\frac{\partial}{\partial \dot{r}_q} \left(\frac{\partial f_{nl,p}}{\partial \dot{r}_i} \phi_{1t,i} \right) = \left(B_{kqi}^p + B_{kqi}^p \right) \dot{r}_k \phi_{1t,i}. \quad (\text{A.12})$$

Concerning the derivative with respect to ω :

$$\begin{aligned} \frac{\partial}{\partial \omega} \frac{\mathbf{F}_{nl}}{\partial \mathbf{c}} \phi_1 &= \mathbf{D} \frac{\partial}{\partial \omega} \left(\frac{\partial \mathbf{f}_{nl}}{\partial \mathbf{r}} \phi_{1t} + \frac{\partial \mathbf{f}_{nl}}{\partial \dot{\mathbf{r}}} \omega \nabla \mathbf{D}^* \phi_{1t} \right) \\ &= \mathbf{D} \frac{\partial \mathbf{f}_{nl}}{\partial \dot{\mathbf{r}}} \omega \nabla \mathbf{D}^* \phi_{1t} \\ &\quad + \mathbf{D} \frac{\partial}{\partial \dot{\mathbf{r}}} \left(\frac{\partial \mathbf{f}_{nl}}{\partial \mathbf{r}} \phi_{1,t} + \frac{\partial \mathbf{f}_{nl}}{\partial \dot{\mathbf{r}}} \dot{\phi}_{1,t} \right) \nabla \mathbf{D}^* \mathbf{c} \end{aligned} \quad (\text{A.13})$$

References

- [1] M. Krack, L. Salles, F. Thouverez, Vibration Prediction of Bladed Disks Coupled by Friction Joints, *Archives of Computational Methods in Engineering* 24 (3) (2017) 589–636. [doi:10.1007/s11831-016-9183-2](https://doi.org/10.1007/s11831-016-9183-2).
- 430 [2] O. V. Gendelman, E. Gourdon, C. H. Lamarque, Quasiperiodic energy pumping in coupled oscillators under periodic forcing, *Journal of Sound and Vibration* 294 (4) (2006) 651–662. [doi:10.1016/j.jsv.2005.11.031](https://doi.org/10.1016/j.jsv.2005.11.031).
- [3] Y. Starosvetsky, O. V. Gendelman, Vibration absorption in systems with a nonlinear energy sink: Non-linear damping, *Journal of Sound and Vibration* 324 (3) (2009) 916–939. [doi:10.1016/j.jsv.2009.02.052](https://doi.org/10.1016/j.jsv.2009.02.052).
- 435 [4] T. Detroux, G. Habib, L. Masset, G. Kerschen, Performance, robustness and sensitivity analysis of the nonlinear tuned vibration absorber, *Mechanical Systems and Signal Processing* 60-61 (2015) 799–809. [doi:10.1016/j.ymsp.2015.01.035](https://doi.org/10.1016/j.ymsp.2015.01.035).
- [5] R. Vigué, G. Kerschen, Nonlinear vibration absorber coupled to a nonlinear primary system: A tuning methodology, *Journal of Sound and Vibration* 326 (3) (2009) 780–793. [doi:10.1016/j.jsv.2009.05.023](https://doi.org/10.1016/j.jsv.2009.05.023).
- 440

- [6] A. F. Vakakis (Ed.), Normal Modes and Localization in Nonlinear Systems, Springer Netherlands, 2001.
- [7] A. H. Nayfeh, D. T. Mook, Nonlinear Oscillations, John Wiley & Sons, 2008.
- 445 [8] W. Lacarbonara, G. Rega, A. H. Nayfeh, Resonant non-linear normal modes. Part I: analytical treatment for structural one-dimensional systems, International Journal of Non-Linear Mechanics 38 (6) (2003) 851–872. doi:10.1016/S0020-7462(02)00033-1.
- [9] M. Monteil, C. Touzé, O. Thomas, S. Benacchio, Nonlinear forced vibrations of thin structures with tuned eigenfrequencies: the cases of 1:2:4 and 1:2:2 internal resonances, Nonlinear Dynamics 75 (1)
450 (2014) 175–200. doi:10.1007/s11071-013-1057-7.
- [10] G. Gobat, L. Guillot, A. Frangi, B. Cochelin, C. Touzé, Backbone curves, Neimark-Sacker boundaries and appearance of quasi-periodicity in nonlinear oscillators: application to 1:2 internal resonance and frequency combs in MEMS, Meccanica 56 (8) (2021) 1937–1969. doi:10.1007/s11012-021-01351-1.
- 455 [11] G. Gobat, V. Zega, P. Fedeli, L. Guerinoni, C. Touzé, A. Frangi, Reduced order modelling and experimental validation of a MEMS gyroscope test-structure exhibiting 1:2 internal resonance, Scientific Reports 11 (1) (2021) 16390. doi:10.1038/s41598-021-95793-y.
- [12] N. Di Palma, B. Chouvion, F. Thouverez, Parametric study on internal resonances for a simplified nonlinear blade model, Submitted for Journal publication (2021).
460 URL <https://hal.archives-ouvertes.fr/hal-03353678>
- [13] A. F. Vakakis, Dynamics of a nonlinear periodic structure with cyclic symmetry, Acta Mechanica 95 (1) (1992) 197–226. doi:10.1007/BF01170813.
- [14] A. F. Vakakis, C. Cetinkaya, Mode Localization in a Class of Multidegree-of-Freedom Nonlinear Systems with Cyclic Symmetry, SIAM Journal on Applied Mathematics 53 (1) (1993) 265–282, publisher: Society for Industrial and Applied Mathematics. doi:10.1137/0153016.
465
- [15] M. King, A. Vakakis, A very complicated structure of resonances in a nonlinear system with cyclic symmetry: Nonlinear forced localization, Nonlinear Dynamics 7 (1) (1995) 85–104.
URL <https://link.springer.com/article/10.1007/BF00045127>

- [16] E. Sarrouy, A. Grolet, F. Thouverez, Global and bifurcation analysis of a structure with cyclic symmetry, *International Journal of Non-Linear Mechanics* 46 (5) (2011) 727–737. doi:10.1016/j.ijnonlinmec.2011.02.005.
- [17] A. Grolet, F. Thouverez, Free and forced vibration analysis of a nonlinear system with cyclic symmetry: Application to a simplified model, *Journal of Sound and Vibration* 331 (12) (2012) 2911–2928. doi:10.1016/j.jsv.2012.02.008.
- [18] A. Grolet, F. Thouverez, Computing multiple periodic solutions of nonlinear vibration problems using the harmonic balance method and Groebner bases, *Mechanical Systems and Signal Processing* 52-53 (2015) 529–547. doi:10.1016/j.ymsp.2014.07.015.
- [19] F. Georgiades, M. Peeters, G. Kerschen, J. C. Golinval, M. Ruzzene, Modal analysis of a nonlinear periodic structure with cyclic symmetry, *AIAA Journal* 47 (4) (2009) 1014–1025. doi:10.2514/1.40461.
- [20] S. Quaegebeur, B. Chouvion, F. Thouverez, L. Berthe, Energy transfer between nodal diameters of cyclic symmetric structures exhibiting polynomial nonlinearities: Cyclic condition and analysis, *Mechanical Systems and Signal Processing* 139 (2020) 106604. doi:10.1016/j.ymsp.2019.106604.
- [21] C. Touzé, M. Amabili, Nonlinear normal modes for damped geometrically nonlinear systems: Application to reduced-order modelling of harmonically forced structures, *Journal of Sound and Vibration* 298 (4) (2006) 958–981. doi:10.1016/j.jsv.2006.06.032.
- [22] C. Touzé, A. Vizzaccaro, O. Thomas, Model order reduction methods for geometrically nonlinear structures: a review of nonlinear techniques, Vol. 105, 2021. doi:10.1007/s11071-021-06693-9.
- [23] H. Poincare, *Les méthodes nouvelles de la mécanique céleste*, Gauthier-Villars et fils., 1893.
- [24] L. Jezequel, C. Lamarque, Analysis of non-linear dynamical systems by the normal form theory, *Journal of Sound and Vibration* 149 (3) (1991) 429–459. doi:10.1016/0022-460X(91)90446-Q.
- [25] D. Hodges, E. Dowell, Nonlinear equations of motion for the elastic bending and torsion of twisted nonuniform rotor blades. Technical Report NASA-TN-D-7818, NASA technical (1974).
- [26] V. Riziotis, S. Voutsinas, D. Manolas, E. Politis, P. Chaviaropoulos, Aeroelastic Analysis of Pre-Curved Rotor Blades, Vol. 2, 2010, Proceedings of the European Wind Energy Conference and Exhibition.

- [27] M. Geradin, D. J. Rixen, Mechanical vibrations: theory and application to structural dynamics, John Wiley & Sons, 2014.
- [28] A. H. Nayfeh, D. T. Mook, L. R. Marshall, Nonlinear Coupling of Pitch and Roll Modes in Ship Motions, *Journal of Hydronautics* 7 (4) (1973) 145–152, publisher: American Institute of Aeronautics and Astronautics. doi:10.2514/3.62949.
- 500 [29] D. L. Thomas, Dynamics of rotationally periodic structures, *International Journal for Numerical Methods in Engineering* 14 (1) (1979) 81–102. doi:10.1002/nme.1620140107.
- [30] M. Mitra, B. I. Epureanu, Dynamic modeling and projection-based reduction methods for bladed disks with nonlinear frictional and intermittent contact interfaces, *Applied Mechanics Reviews* 71 (5), publisher: American Society of Mechanical Engineers Digital Collection (Sep. 2019). doi:10.1115/1.4043083.
- 505 [31] S. Idelsohn, A. Cardona, A reduction method for nonlinear structural dynamic analysis, *Computer Methods in Applied Mechanics and Engineering* 49 (3) (1985) 253–279. doi:10.1016/0045-7825(85)90125-2.
- 510 [32] P. M. A. Slaats, J. de Jongh, A. A. H. J. Sauren, Model reduction tools for nonlinear structural dynamics, *Computers & Structures* 54 (6) (1995) 1155–1171. doi:10.1016/0045-7949(94)00389-K.
- [33] G. Haller, S. Ponsioen, Nonlinear normal modes and spectral submanifolds: existence, uniqueness and use in model reduction, *Nonlinear Dynamics* 86 (3) (2016) 1493–1534. doi:10.1007/s11071-016-2974-z.
- 515 [34] M. Mignolet, A. Przekop, S. Rizzi, S. Spottswood, A review of indirect/non-intrusive reduced order modeling of nonlinear geometric structures, *Journal of Sound and Vibration* 332 (10) (2013) 2437–2460. doi:10.1016/j.jsv.2012.10.017.
- [35] C. Touzé, A normal form approach for nonlinear normal modes, *Research Report Publications du LMA*, numéro 156, LMA (Jan. 2003).
- 520 [36] A. Opreni, A. Vizzaccaro, A. Frangi, C. Touzé, Model order reduction based on direct normal form: application to large finite element MEMS structures featuring internal resonance, *Nonlinear Dynamics* 105 (2) (2021) 1237–1272. doi:10.1007/s11071-021-06641-7.

- [37] S. W. Shaw, C. Pierre, Normal Modes for Non-Linear Vibratory Systems, *Journal of Sound and Vibration* 164 (1) (1993) 85–124. doi:10.1006/jsvi.1993.1198.
- 525 [38] A. Vizzaccaro, Y. Shen, L. Salles, J. Blahoš, C. Touzé, Direct computation of nonlinear mapping via normal form for reduced-order models of finite element nonlinear structures, *Computer Methods in Applied Mechanics and Engineering* 384 (2021) 113957. doi:10.1016/j.cma.2021.113957.
- [39] M. Krack, J. Gross, Theory of harmonic balance, in: *Harmonic Balance for Nonlinear Vibration Problems*, Mathematical Engineering, Springer International Publishing, Cham, 2019, pp. 11–46.
530 doi:10.1007/978-3-030-14023-6_2.
- [40] M. Peeters, R. Vigié, G. Sérandour, G. Kerschen, J. C. Golinval, Nonlinear normal modes, Part II: Toward a practical computation using numerical continuation techniques, *Mechanical Systems and Signal Processing* 23 (1) (2009) 195–216. doi:10.1016/j.ymsp.2008.04.003.
- [41] L. Xie, S. Baguet, B. Prabel, R. Dufour, Bifurcation tracking by Harmonic Balance Method for performance tuning of nonlinear dynamical systems, *Mechanical Systems and Signal Processing* 88 (2017)
535 445–461. doi:10.1016/j.ymsp.2016.09.037.
- [42] T. Detroux, L. Renson, L. Masset, G. Kerschen, The harmonic balance method for bifurcation analysis of large-scale nonlinear mechanical systems, *Computer Methods in Applied Mechanics and Engineering* 296 (2015) 18–38. doi:10.1016/j.cma.2015.07.017.
- 540 [43] R. Seydel, *Practical Bifurcation and Stability Analysis*, 3rd Edition, Interdisciplinary Applied Mathematics, Springer-Verlag, New York, 2010.
- [44] Y. Kuznetsov, *Elements of Applied Bifurcation Theory*, 3rd Edition, Applied Mathematical Sciences, New York, 2004, Springer-Verlag. doi:10.1007/978-1-4757-3978-7.
- [45] F. Fontanela, A. Grolet, L. Salles, N. Hoffmann, Computation of quasi-periodic localised vibrations in nonlinear cyclic and symmetric structures using harmonic balance methods, *Journal of Sound and*
545 *Vibration* 438 (2019) 54–65. doi:10.1016/j.jsv.2018.09.002.
- [46] G. Floquet, Sur les équations différentielles linéaires à coefficients périodiques, *Annales scientifiques de l'École Normale Supérieure* 2e série, 12 (1883) 47–88. doi:10.24033/asens.220.

- 550 [47] A. Nayfeh, B. Balachandran, Applied Nonlinear Dynamics: Analytical, Computational and Experimental Methods, New York, 1995, wiley VCH.
- [48] C. Touzé, O. Thomas, M. Amabili, Transition to chaotic vibrations for harmonically forced perfect and imperfect circular plates, International Journal of Non-Linear Mechanics 46 (1) (2011) 234–246. [doi:10.1016/j.ijnonlinmec.2010.09.004](https://doi.org/10.1016/j.ijnonlinmec.2010.09.004).
- 555 [49] T. M. Cameron, J. H. Griffin, An alternating frequency/time domain method for calculating the steady-state response of nonlinear dynamic systems, Journal of Applied Mechanics 56 (1) (1989) 149–154. [doi:10.1115/1.3176036](https://doi.org/10.1115/1.3176036).